Biomaterials 31 (2010) 5986–5995

Contents lists available at ScienceDirect

Biomaterials

journal homepage: www.elsevier.com/locate/biomaterials

Amyloid hydrogel derived from curly protein fibrils of α-synuclein

Ghibom Bhak [a], Soonkoo Lee [a], Jae Woo Park [a], Sunghyun Cho [b], Seung R. Paik [a,*]

[a] School of Chemical and Biological Engineering, College of Engineering, Seoul National University, 599 Gwanak-Ro, Gwanak-Gu, Seoul 151 744, Republic of Korea
[b] Department of Computer Science and Engineering, Pohang University of Science and Technology, Pohang, Gyeongbuk 790 784, Republic of Korea

ARTICLE INFO

Article history:
Received 29 January 2010
Accepted 29 March 2010
Available online 14 May 2010

Keywords:
Self-assembly
Amyloidogenesis
Hydrogel
Protein nanofibrils
Nanomatrix

ABSTRACT

Elucidation of molecular assembly mechanism of protein-based suprastructure formation is pivotal to develop biomaterials. A single amyloidogenic protein of α-synuclein turned into two morphologically distinctive amyloid fibrils – 'curly' (CAF) vs. 'straight' (SAF) – depending on its fibrillation processes. Mutually exclusive production of CAF and SAF was achieved with either centrifugal membrane filtration of the preformed oligomeric species of α-synuclein or agitated incubation of its monomeric form, representing amyloidogeneses via double-concerted and nucleation-dependent fibrillation model, respectively. Differences in secondary structures of CAF and SAF have been suggested to be responsible for their morphological uniqueness with structural flexibility and mechanical strength. Both polymorphs exerted the self-propagation property, demonstrating that their characteristic morphologies were inherited for two consecutive generations to daughter and granddaughter fibrils through the seed-dependent fibrillation procedure. Accumulation of CAF produced amyloid hydrogel composed of fine nano-scaled three-dimensional protein fibrillar network. The hydrogel made of daughter CAF was demonstrated to be a suitable nanomatrix for enzyme entrapment, which protected the entrapped enzyme of horseradish peroxidase from loss of activity due to multiple catalyses and heat treatment. The nano-scaled fibrillar network of CAF, therefore, could exhibit a full potential to be further applied in the promising areas of nanobiotechnology including tissue engineering, drug delivery, nanofiltration and biosensor development.

1. Introduction

Protein-based suprastructure formation is one of key phenomena involved in a diverse range of biological activities from normal cellular biogenesis to pathogenesis of various degenerative disorders. These suprastructures are also suggested to be engineered *in vitro* to provide biologically compatible materials [1]. Therefore, elucidation of molecular assembly mechanism for the suprastructure formation is crucial not only to understand its implications in biology but also to obtain biomaterials for their eventual applications in the area of nanobiotechnology.

Amyloid fibrils are highly ordered fibrillar protein aggregates known to be stabilized predominantly by cross-β-sheet conformation [2]. They are the product of disorder-to-order transition of partially misfolded proteins through selective molecular self-assembly process [3]. Mature amyloid fibrils elicit polymorphism resulted from either molecular-level structural variations of individual amyloidogenic proteins or alterations in intra- or inter-fibrillar interactions [4]. This amyloid formation has been closely associated with neurodegenerative disorders including Parkinson's disease (PD), Alzheimer's disease (AD), and Prion disease [5] although toxic cause of the cellular degeneration remains unsettled [6]. The amyloid fibrils exhibit biological activities such as biofilm formation of enterobacteria, hyphae formation of fungi, egg envelope formation of insects and fish, biosynthesis of melanin within mammalian melanocytes and activation of factor XII in human hemostasis [7,8]. In addition, the amyloid fibrils are also considered as protein nanofibrils with an average width of 10–20 nm and a mechanical strength comparable to spider silk [9]. This nano-scaled biomaterial has been suggested to have a full potential for applications by providing functional templates for conductive nanowire preparation, nanoparticle alignment and enzyme immobilization and by turning into liquid crystal state and hydrogel formation [10]. Exploration of diversified amyloid fibrillation procedures, therefore, will bring us practical means to obtain various functional nanomaterials for biotechnological applications.

Molecular self-assembly mechanism for the amyloidogenesis has been prevalently modeled with the nucleation-dependent fibrillation process [11–13]. After thermodynamically unfavorable nucleus formation, the fibrillation process is facilitated by accreting monomeric units in either pre-structured or unstructured form to exhibit template complementarity, which has been reflected on the

* Corresponding author. Tel.: +82 2 880 7402; fax: +82 2 888 1604.
E-mail address: srpaik@snu.ac.kr (S.R. Paik).

0142-9612/$ – see front matter © 2010 Elsevier Ltd. All rights reserved.
doi:10.1016/j.biomaterials.2010.03.080

fibrillation kinetics showing a lag phase followed by an exponential growth phase during agitated incubation of amyloidogenic proteins [14]. Recently, however, we have proposed another model named the double-concerted fibrillation to parallel the nucleation-dependent model by investigating a dramatically accelerated amyloidogenesis of α-synuclein [15], a pathological component of Parkinson's disease by participating in the Lewy body formation [16]. α-synuclein is a presynaptic protein with undefined physiological function although its involvement in synaptic plasticity has been suggested [17]. The protein could be divided into three regions in its primary structure. The N-terminal region (residues 1–60) has been demonstrated to form amphipathic α-helices upon membrane interaction. The hydrophobic middle segment (residues 61–95) is also known as the non-Aβ component of Alzheimer's disease amyloid. The protein ends with the acidic C terminus (residues 96–140), which is most variable among other synuclein isoforms including β- and γ-synucleins. The protein has been known to be a "natively unfolded" protein [18]. When incubated *in vitro*, α-synuclein tends to form amyloid fibrils in which the unstructured protein has aligned to form cross-β-sheet conformation [19,20]. According to our double-concerted model, the oligomeric granular species of α-synuclein obtained in the middle of lag phase during its *in vitro* fibrillation process act as a growing unit for the fibrillation following a subtle structural rearrangement within the preformed oligomeric structures induced by either shear stress or organic solvent treatment [15,21]. In this report, we demonstrate that both models are indeed operative in the fibrillation of α-synuclein by showing self-propagating molecular-level polymorphism of the resulting amyloid fibrils between 'straight' versus 'curly' polymorphs. The curly fibrils obtained via the double-concerted fibrillation process produce a hierarchical superstructure of amyloid hydrogel which provides a three-dimensional nano-scaled protein fibrillar meshwork optimal for the enzyme entrapment of horseradish peroxidase.

2. Materials and methods

2.1. Preparation of α-synuclein

Recombinant human α-synuclein was prepared as the procedure previously described [22]. Briefly, human α-synuclein gene cloned in pRK172 was overexpressed in *Escherichia coli* BL21 (DE3). Subsequent cell lysate was heat-treated and applied to DEAE-Sephacel anion-exchange, Sephacryl S-200 size-exclusion and S-Sepharose cation-exchange chromatography. Completely purified α-synuclein was stored in aliquots at −80 °C following dialysis against total 6 L of 20 mM Mes at pH 6.5 with 3 times of buffer change.

2.2. Polymorphic amyloid fibril formation of 'curly' and 'straight' amyloid fibrils of α-synuclein

Two types of polymorphic amyloid fibrils are obtained with following procedures [15]. For 'curly' amyloid fibrils (CAF), α-synuclein granules were subjected to the repetitive centrifugal membrane filtrations using Microcon YM-30 (Millipore) with Centrifuge 5415R (Eppendorf, Germany) at 14,000*g* at 37 °C. Following each filtration for 2 min, the filtrate was combined to the original sample, and subjected to another round of the filtration. The resulting CAF were collected via a reverse centrifugation after resuspension with the same initial volume of 20 mM Mes at pH 6.5. The oligomeric granules of α-synuclein were obtained in the middle of the lag phase of the aggregation kinetics assessed with thioflavin-T binding fluorescence. Normal agitated fibrillation of α-synuclein (1 mg/ml) was carried out in 20 mM Mes (pH 6.5) at 37 °C with a continuous shaking on an orbit shaker at 200 rpm. Prolonged incubation of α-synuclein under the agitated condition resulted in the formation of 'straight' amyloid fibrils (SAF).

2.3. Transmission electron microscope (TEM)

An aliquot containing amyloid fibrils of α-synuclein was adsorbed onto a carbon-coated 200-mesh copper grid (Ted Pella Inc., USA). Following negative staining of air-dried sample with 2% uranyl acetate (Electron Microscopy Sciences, USA) for 20 s, the amyloid fibrils were visualized with TEM (JEM 1010, Jeol, Japan).

2.4. Atomic force microscope (AFM)

Morphologies of α-synuclein amyloids were examined with AFM (Dimension 3100, Veeco, USA). After adsorption of the α-synuclein amyloids on freshly cleaved mica, the mica surface was washed with excess volume of double-distillated water (Direct-Q, Millipore, USA). The completely air-dried samples were analyzed with AFM in tapping mode.

2.5. Statistical analysis of persistence length of the amyloid fibrils of CAF and SAF

Amyloid fibrils visualized with AFM were traced by using an algorithm developed for obtaining the contour length (C_L) and the end-to-end distance in two dimensions (R_{2D}). The structures of amyloid fibrils have reached equilibrium on the mica surface before being adsorbed [23]. Since the structural fluctuations reflect mechanical properties of the fibrils, the statistical mechanics of the worm-like chain model for semiflexible polymers has been employed to evaluate the persistence length [24] which indicates the fibrillar stiffness. The persistence length (P) was determined from a statistical relationship between C_L and R_{2D} of a polymer chain according to the following equation (1) [23,25].

$$\left\langle R^2 \right\rangle_{2D} = 4PC_L\left(1 - \frac{2P}{C_L}\left(1 - e^{-C_L/2P}\right)\right) \quad (1)$$

2.6. Attenuated total reflectance-Fourier transformation infrared (ATR-FTIR) spectrophotometer

Both CAF and SAF were resuspended in 20 mM Mes at pH 6.5. Each amyloid fibril sample was placed on a Zinc Selenide (ZnSe) ATR crystal. ATR spectra were recorded on a Nicolet 6700 FTIR spectrometer equipped with a DTGS detector (Thermo Scientific, USA) with a spectral resolution of 4 cm^{-1}. Data fitting and curve deconvolution for ATR-FTIR spectra were performed using OriginPro 7.5 software (OriginLab).

2.7. Self-propagation experiments of polymorphic amyloid fibrils

Seeds for the fibrillar growth to obtain daughter and granddaughter fibrils were prepared by ultrasonication of the mature amyloid fibrils using a micro-tip-type ultrasonic processor (VCX 750, Sonics & Materials, Inc., USA) at frequency of 20 kHz and power output of 750 W. Sonication was performed repeatedly with the sample located on ice. Each cycle consisted of an on/off cycle for 5 s each. After each 5 cycles of sonication, the sample was quiescently placed on ice for 1 min in the absence of sonication. The resulting amyloid fragments obtained with overall 40 cycles of ultrasonication were examined with TEM and used as the seeds for subsequent fibrillar growth. Daughter fibrils were grown under a quiescent condition by seeding monomeric solution in the presence of 5% of the sonicated fragments. Daughter fibrils were also used for the seed preparation to obtain granddaughter fibrils under a quiescent condition.

2.8. Field-emission scanning electron microscope (FE-SEM)

For the SEM analysis, hydrogel samples were prepared according to a previously described cryofixation, cryofracturing and freeze-drying method [26]. Swollen and freeze-dried hydrogels were sputter-coated with gold/palladium (approximately 5 nm of thickness) using Emscope SC 400 (Electron Microscopy Sciences, USA). The interior and surface structures of hydrogels were examined with FE-SEM (SUPRA 55VP, Carl Zeiss, Germany) at 2.0 kV.

2.9. Confocal laser scanning microscope (CLSM)

Confocal images of the hydrogel stained with thioflavin-T were obtained with CLSM (LSM510, Carl Zeiss, Germany). The thioflavin-T binding fluorescence of the amyloid fibrils within the hydrogel was examined at BP (bandpass filter) 475–525 nm with excitation at 458 nm.

2.10. Amyloid hydrogel preparation and entrapment of horseradish peroxidase (HRP) within the hydrogel

Amyloid hydrogel was directly prepared with the centrifugal membrane filtration process. Transparent hydrogels were obtained on the filter membrane of Microcon YM-30 after approximately 20 times of the repetitive filtrations of α-synuclein granules at 2 mg/ml in 20 mM Mes, pH 6.5. On the other hand, the hydrogel for the enzyme entrapment of HRP (Sigma, USA) was prepared with the daughter fibrils of CAF. The mixture of preformed daughter CAF and HRP was subjected to the centrifugal membrane filtration at 14,000*g* until the solution passed through the membrane. HRP of 1 μg was used to combine with the daughter CAF of 2 mg in 20 mM Mes, pH 6.5 in order to prepare the HRP-entrapped hydrogel. After collecting the HRP-hydrogel via a reverse centrifugation, the hydrogel was fully swollen in 20 mM Mes at pH 6.5 for 1 h. For the removal of free HRP unbound to or released from the hydrogel, the HRP-entrapped hydrogel was washed over 10 times with fresh 20 mM Mes buffer. Enzymatic activity of the entrapped HRP within the

hydrogel was monitored with 3,3′,5,5′-tetramethylbenzidine (TMB) Liquid Substrate System (Sigma, USA) by using UV/Visible Spectrophotometer (Ultrospec™ 2100 *pro*, Amersham Biosciences, England).

3. Results

3.1. Polymorphic amyloid fibril formation of α-synuclein

Intriguingly, two polymorphic amyloid fibrils were derived from a single amyloidogenic protein of α-synuclein by altering fibrillation procedures between an agitated incubation of monomers and a centrifugal membrane filtration of the oligomeric granular species, which represent the nucleation-dependent fibrillation and the double-concerted fibrillation, respectively [15] (Fig. 1). Under normal agitated incubation at 200 rpm and 37 °C for 100 h, α-synuclein turned into 'straight' amyloid fibrils (SAF) with an average width of 15.2 nm as routinely observed in most *in vitro* amyloidogeneses (Fig. 1A, top). These fibrils remained interacted with each other at acute angles and stayed in a less entangled state (Fig. 1A, bottom). On the other hand, however, 'curly' amyloid fibrils (CAF) of the same α-synuclein were evidently generated (Fig. 1B, top) following a single centrifugal membrane filtration (Microcon YM-30) for 12 min of centrifugation at 14,000*g* and 37 °C with the oligomeric granular species of α-synuclein. The oligomeric species were collected at 17-h time point in the middle of lag phase of the normal agitated incubation of soluble α-synuclein at 1 mg/ml in 20 mM Mes, pH 6.5 [15] (see Fig. S1). Only 12 min of the centrifugal membrane filtration turned out to be

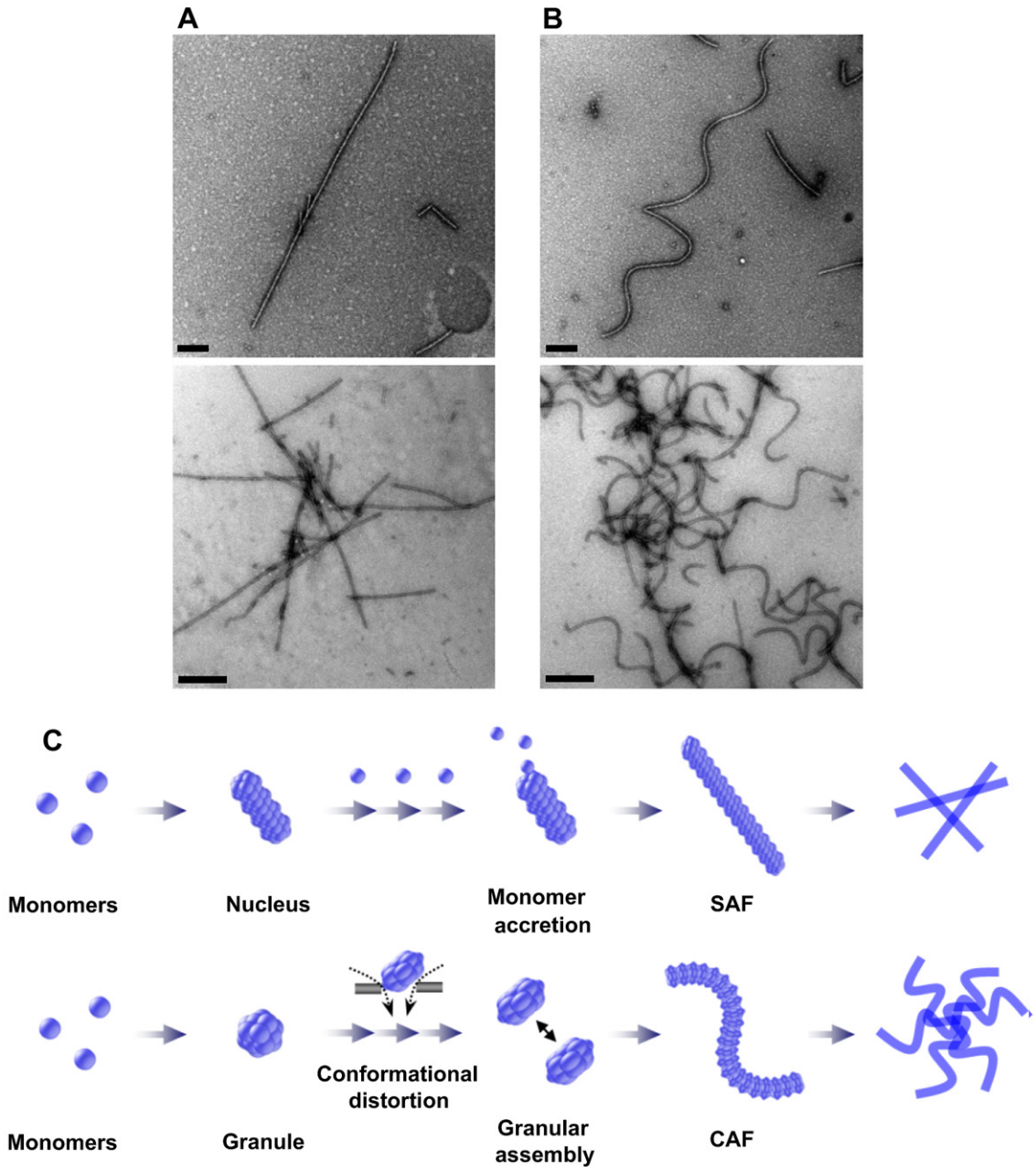

Fig. 1. Two distinctive polymorphic amyloid fibrils derived from a single protein of α-synuclein. A, Negatively stained TEM images of SAF produced via the agitated incubation of monomeric α-synuclein at 37 °C. Each scale bar represents 0.2 μm (top) and 0.5 μm (bottom). B, TEM images of CAF generated by the centrifugal membrane filtration of the oligomeric granular species of α-synuclein with Microcon YM-30 at 14,000g and 37 °C. Scale bars represent 0.2 and 0.5 μm for the top and bottom panels, respectively. C, Schematic representation of amyloidogenesis depicted for the nucleation-dependent (top row) and the double-concerted fibrillation model (bottom row).

sufficient to produce the morphologically distinct CAF whereas SAF were produced after hours of the agitated incubation. The CAF enriched with repetitive centrifugal filtrations for 20 times of a 2-min filtration cycle gave rise to a fibrillar network where the fibrils were interacted at obtuse angles and heavily entangled (Fig. 1B, bottom). Schematic representation (Fig. 1C) summarizes the two discrete fibrillation processes of the nucleation-dependent (top) and the double-concerted (bottom) fibrillations, which result in two morphologically distinctive amyloid fibrils of SAF and CAF from the single protein of α-synuclein, respectively. In the nucleation-dependent model, the nucleation center acts as a template for the soluble monomeric protein for rather extended period of time by directing conformational transition of the accreting protein for the production of insoluble SAF. On the other hand, CAF are rapidly produced via the granular assembly following conformational distortion of the preformed oligomeric granular species in the presence of shear stress imposed by the centrifugal filtration [15]. It is the particulate state of the oligomeric species that becomes sensitive to the physical influence of shear stress.

3.2. Biophysical and biochemical analyses of polymorphs

Biophysical and biochemical properties of CAF were examined in comparison with SAF to reveal fibrillar flexibility/strength, structural characteristics, and self-propagating property. Fibrillar flexibility of the amyloid fibrils was evaluated for both CAF and SAF with an algorithm developed for estimating contour length (C_L) and end-to-end distance of individual fibril in two dimensions (R_{2D}) [23,25]. AFM images of more than 50 fibrils of each polymorph formed on the mica surface were traced and subjected to the algorithmic analysis (Fig. 2A). As shown in the plot of C_L and R_{2D} distributions (Fig. 2B), the maximum C_L of mature CAF was 6.0 μm while the maximum C_L of SAF was 3.2 μm, indicating that CAF were overgrown to SAF by approximately two times in length. The C_L and R_{2D} of SAF were almost identical, meaning that those fibrils were indeed straight in their morphology (Fig. 2B, ○). On the other hand, the R_{2D} values of CAF, in spite of their scattered distribution, were much shorter than their C_L, suggesting the curly state of the fibrils (Fig. 2B, ●). Statistical analyses of C_L and R_{2D} also revealed that average persistence length (P_{av}) of two polymorphs exhibited a startling difference in more than three orders of magnitude (Fig. 2B, inset). CAF appeared to be highly flexible based on the P_{av} value of 1.7×10^{-1} μm (Fig. 2B inset, ●), whereas SAF were shown to be considerably stiff with P_{av} of 1.4×10^{2} μm (Fig. 2B inset, ○). It would be the flexibility of CAF that affords an outstanding property of a breakage resistance of the fibrils against shear stress imposed by the centrifugal membrane filtration (Fig. 2C). The final structures of CAF were maintained even after 30 times of the repetitive filtrations with a 5-min cycle (Fig. 2C, top row). In the case of SAF, however, most of them were broken into fragments after the same number of repetitive filtrations (Fig. 2C, bottom row). This data apparently indicated that the CAF fragmentation was unlikely to occur during the filtration-induced amyloidogenesis process; thus the fragmentation process was not included in the double-concerted fibrillation model (Fig. 1C). The mechanical strength of CAF was also compared with that of SAF with an intermittent sonication treatment for 20 cycles with an on/off cycle of 3 s each (Fig. 2D). The resulting fibrils/fragments were also analyzed with the same algorithm employed above. Although the C_L distribution of CAF became broader to some degree after the sonication treatment, most of their C_L remained unaffected (Fig. 2D, top row). On the other hand, almost all the SAF were degraded into small fragments of approximately 300 nm in average length from their original length of 3.4 μm (Fig. 2D, bottom row). Taken together, CAF have been demonstrated to be much stronger than SAF, which could raise their potential for future applications.

Structural signature of CAF was compared with that of SAF by employing the attenuated total reflectance Fourier transformation infrared (ATR-FTIR) spectrophotometer. Analysis of the amide I profile (1600–1700 cm^{-1}) has been often used to determine secondary structures of proteins. Especially in the case of amyloid fibrils, ATR-FTIR has been employed to find their parallel or antiparallel β-sheet patterns in many researches [27–31]. Deconvolution of the spectra of SAF and CAF at the amide I region yielded discrete patterns of their constituting 5 different components at 1619, 1630, 1650, 1668, and 1683 cm^{-1} (Fig. 2E and F). Assignment of the secondary structures for the components and their relative contributions to overall spectra of SAF and CAF are presented in Table 1. The SAF spectrum gave rise to the major peak at 1630 cm^{-1} with % contribution of 43.3%, representing parallel β-sheet conformation (Fig. 2E) [27,28]. It also contained antiparallel β-sheet structure as it was monitored at 1619 and 1683 cm^{-1} with the relative contributions of 19.9% and 3.5%, respectively [27,28,30]. These β-sheet structures were accompanied by β-turns at 1668 cm^{-1} with 19.5%. The remaining part consisted of either α-helix or random coil collectively observed at 1650 cm^{-1} by 13.8%. In the case of CAF, on the other hand, the major peak at 1630 cm^{-1} decreased significantly to 23.9% while the peaks at 1619, 1650, and 1683 cm^{-1} increased considerably to 29.8%, 21.3%, and 6.1%, respectively (Fig. 2F). These data elucidate that the antiparallel β-sheet structure became prominent for CAF along with a concomitant alteration in α-helix/random coil while SAF contained the parallel β-sheet conformation predominantly. Difference in the content of the secondary structures, therefore, defines the molecular-level polymorphism of SAF and CAF.

3.3. Self-propagation of amyloid fibrils

To elaborate a typical characteristic of amyloidogenesis, self-propagation property of the amyloid polymorphs of CAF and SAF was investigated by incubating monomeric α-synuclein with the seeds obtained from the two types of fibrils following two consecutive generations of fibrillation (Fig. 3A) [4]. Sonicated fragments of both parent CAF and SAF were used to seed daughter fibril growth, which was followed by another round of the sonication-induced seed production and fibril growth in the presence of monomeric α-synuclein for granddaughter fibril formation (Fig. 3A). Under normal quiescent incubation in the presence of the seeds at 5%, all the fibrillations were dramatically enhanced compared with non-seeded incubation of the monomeric protein (data not shown). In the presence of the sonicated fragments of parent CAF, the daughter fibrils inherited the wavy surface structure of the parent CAF. The curly morphology of daughter fibrils was also transmitted for another generation to the granddaughter fibrils (Fig. 3B, top row). For SAF, their daughter and granddaughter fibrils also inherited the straight fibrillar morphology of the parent SAF as revealed in TEM images (Fig. 3B, bottom row). The seeds, therefore, determined the final morphologies of mature amyloid fibrils in next generations. It is the transmission of morphological heritage of parent amyloid fibrils that substantiates the self-propagating nature of polymorphic amyloid fibrils of CAF and SAF by retaining their molecular characteristics.

3.4. Amyloid hydrogel

Remarkably, only the CAF turned into a hierarchical superstructure of amyloid hydrogel via extensive three-dimensional fibrillar meshwork formation. This hydrogel formation was achieved exclusively with the centrifugal membrane filtration of

α-synuclein granules. Initially, small pieces of hydrogel formed after more than 5 times of the repetitive filtrations with 2 min-cycle. As the number of filtrations increased, those pieces combined into a lump of hydrogel on the membrane. Its solidity was demonstrated with the hydrogel located on the surface of a tilted glass slide (Fig. 4A). Optical transparency of the hydrogel was revealed on the top of the blue emblem (Fig. 4B). Presence of amyloid fibrils within the hydrogel was assessed with thioflavin-T binding fluorescence and visualized with confocal laser scanning microscope (CLSM) at BP (bandpass filter) 475–525 nm with

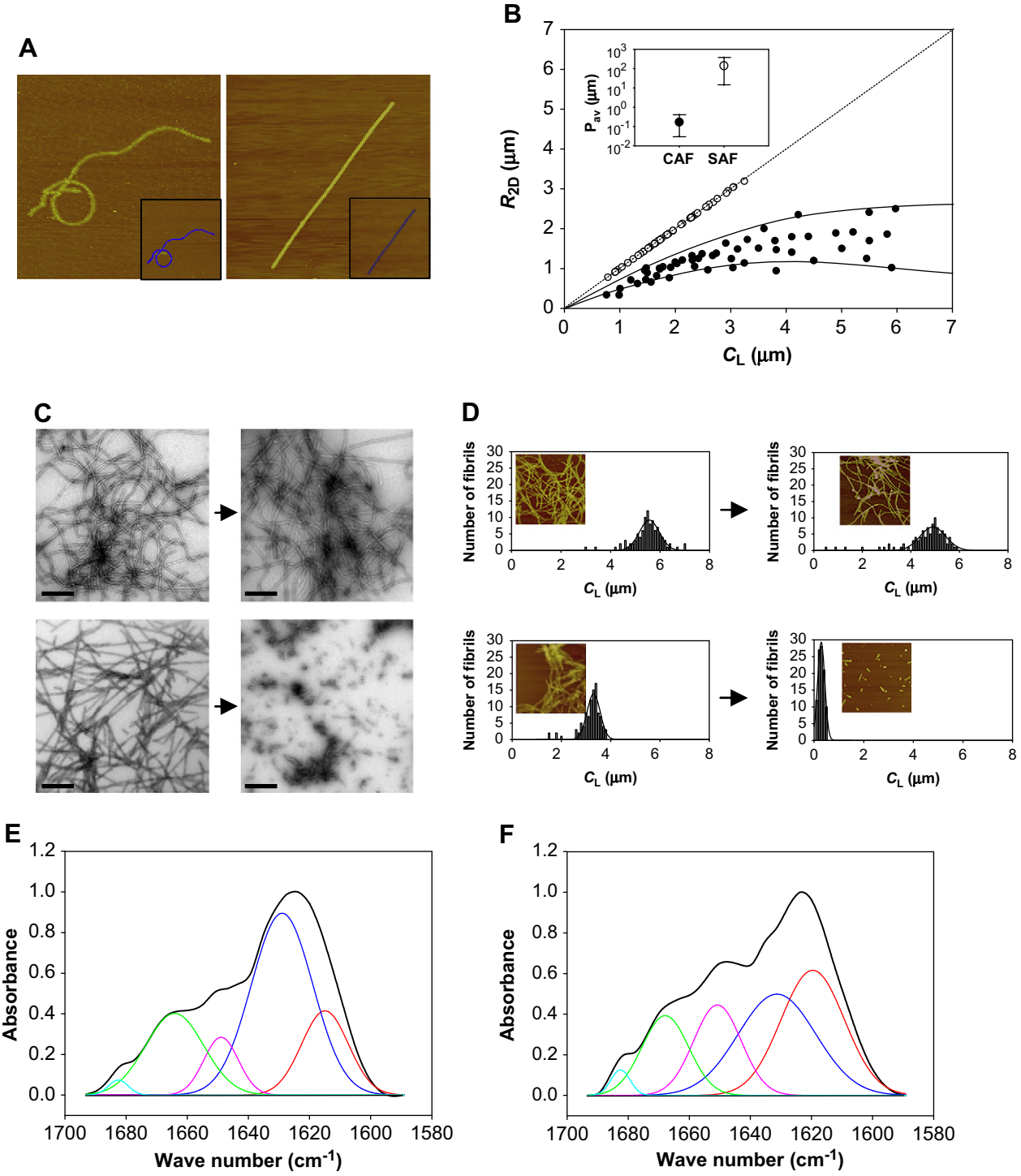

Fig. 2. Biophysical and biochemical properties of CAF and SAF. A, AFM images (2.5 μm × 2.5 μm) of a single fibril of CAF (left) and SAF (right). Traced image of each amyloid fibril is shown in the inset. B, Plot of R_{2D} and C_L of CAF (●) and SAF (○). Average persistence length (P_{av}) of CAF (●) and SAF (○) are presented in the inset. C, Breakage resistance of CAF (top row) and SAF (bottom row) against shear stress imposed by the centrifugal membrane filtration. Arrow distinguishes two TEM images between before and after the repetitive filtrations. All the scale bars indicate 0.5 μm. D, The C_L distributions of CAF (top row) and SAF (bottom row) before and after the 20 on/off cycles (3 s each for on/off) of intermittent ultrasonication treatment. AFM morphologies (5 μm × 5 μm) of the fibrils/fragments are also provided in the insets. Arrows indicate the ultrasonication process. ATR-FTIR spectra (bold line) of the amide I band of SAF (E) and CAF (F) are presented. Color lines obtained via spectral deconvolution represent the constituting secondary structures of the polymorphs (see Table 1).

Table 1
Relative contribution of secondary structures in the amide I bands of ATR-FTIR spectra of CAF and SAF.

Secondary structure	Amide I wave number (cm^{-1})	Relative contribution (% ± S.D.)	
		SAF	CAF
Antiparallel β-sheets	1683	3.5 ± 0.3	6.1 ± 0.2
β-Turns	1668	19.5 ± 1.6	18.9 ± 1.4
α-Helices and/or random coils	1650	13.8 ± 1.0	21.3 ± 1.2
Parallel β-sheets	1630	43.3 ± 1.7	23.9 ± 1.8
Antiparallel β-sheets	1619	19.9 ± 1.1	29.8 ± 0.7

excitation at 458 nm (Fig. 4C). Its optical image was also shown (Fig. 4D). To depict pore size of the amyloid hydrogel, a field emission scanning electron microscopy (FE-SEM) was employed to reveal a well-defined fibrillar network of the hydrogel (Fig. 4E). The hydrogel samples were prepared by cryofixation, cryofracturing and freeze-drying method [26,32], by which water inside hydrogel can be eliminated with minimal disruption of the fibrillar network. From the SEM analysis, average pore size was determined as approximately 52.9 nm with the pore size distribution shown in Fig. S2.

3.5. Enzyme entrapment

To take advantage of the fine nanospace within the three-dimensional fibrillar network, the amyloid hydrogel was pursued to serve a matrix for enzyme entrapment as an example of its undefined but promising future applications. In fact, horseradish peroxidase (HRP) was entrapped within the hydrogel by mixing HRP (1 μg) and the preformed daughter CAF (2 mg) obtained from the self-propagation experiment (Fig. 3), which was followed by

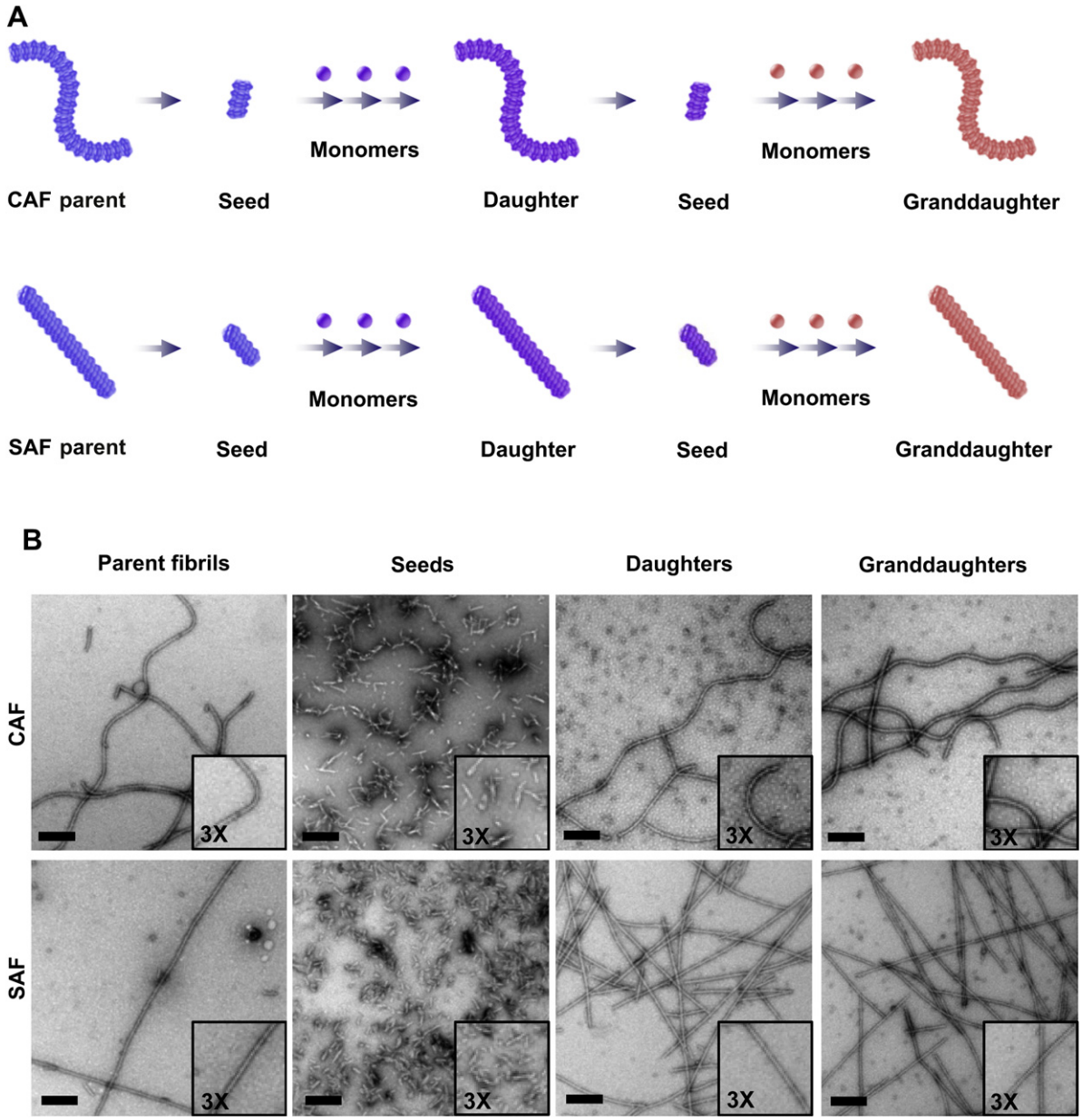

Fig. 3. Self-propagating nature of the two amyloid polymorphs. A, Schematic representation of the self-propagation processes of CAF (top row) and SAF (bottom row). Distinct morphology of each polymorph is inherited to its progenies by the accretion of monomeric α-synuclein to the parental fragments. B, TEM images of CAF (top row) and SAF (bottom row) from the parent amyloid fibrils to their granddaughter fibrils. Magnified images by three-fold for the fibrils are also presented in the insets. The scale bars represent 0.2 μm.

performing the centrifugal filtration using Microcon YM-30 until all the solvent passed through the membrane. After swelling the hydrogel in 20 mM Mes at pH 6.5 for 1 h, the hydrogel was thoroughly washed for over 10 times with the fresh buffer. The substrate of 3,3′,5,5′-tetramethylbenzidine (TMB) was then added to the hydrogel. The blue color was developed almost instantaneously within 5 s only from the HRP-entrapped hydrogel (Fig. 5A, bottom row). The oxidation product of TMB was also monitored

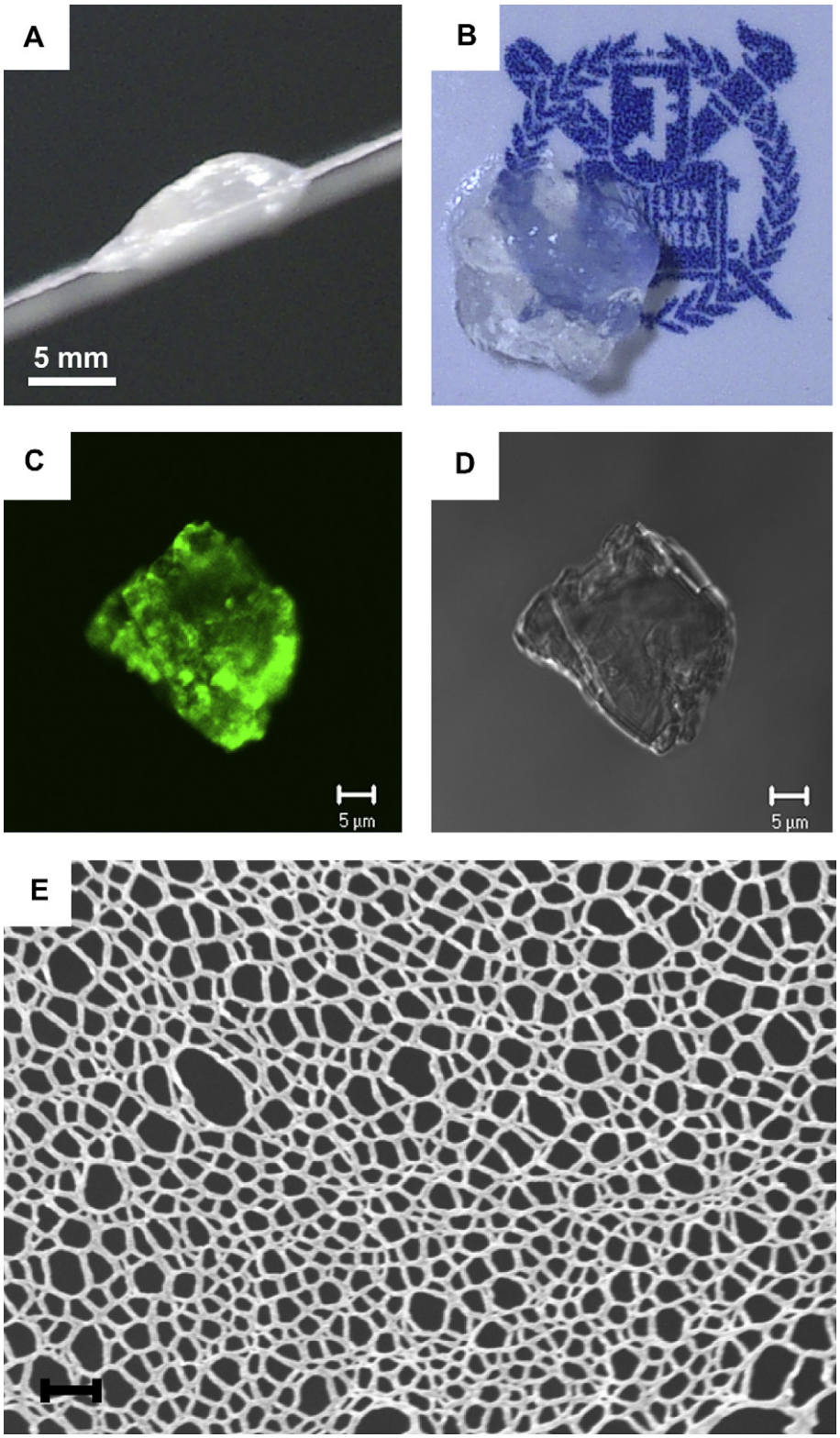

Fig. 4. Amyloid hydrogel of CAF. A, The hydrogel stabilized on the surface of a tilted glass slide is shown. B, Optical transparency of the hydrogel revealed on the top of the blue emblem of Seoul National University. C, Thioflavin-T binding fluorescence of the amyloid fibrils within the hydrogel is visualized with CLSM. D, Optical image of the amyloid hydrogel examined in the panel (C). E, FE-SEM image of the freeze-dried amyloid hydrogel revealing a well-defined nano-scaled fibrillar network. The scale bar indicates 0.2 μm.

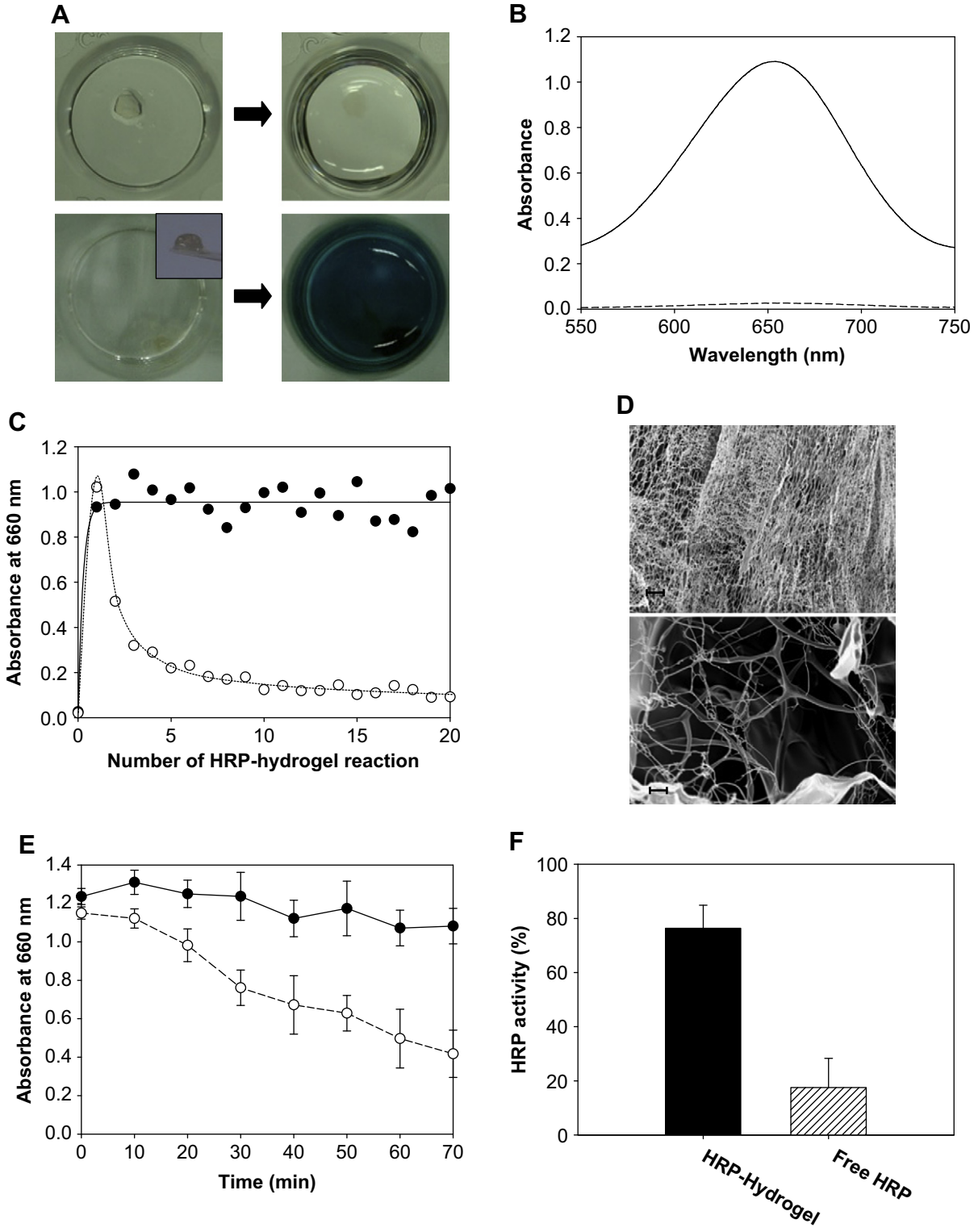

Fig. 5. HRP entrapment within the amyloid hydrogel. A, Development of blue color representing the oxidation of TMB by HRP is shown for the HRP-entrapped amyloid hydrogel (bottom row) while the CAF hydrogel lacking HRP fails to produce the blue color (top row). The HRP-containing stable hydrogel is also presented in the inset (bottom row). B, Absorbance spectra of TMB are demonstrated after incubation with the hydrogels with (solid line) and without (dashed line) HRP. C, The HRP activities are monitored during multiple catalyses for the enzymes entrapped within the amyloid hydrogel (closed dots) and the collagen-based hydrogel (open dots). D, Appearance of pores of the CAF amyloid hydrogel (top) and the collagen hydrogel (bottom) examined with FE-SEM (scale bar = 1 μm). E, Protection of HRP during thermal inactivation at 60 °C was assessed for the enzyme either entrapped within the amyloid hydrogel (closed dots) or free in solution (open dots). The HRP activity was monitored with UV/VIS spectrophotometer by observing absorbance at 660 nm. F, Retention of the enzymatic activity of HRP either entrapped within the hydrogel (black bar) or free in solution (oblique bar) was evaluated after a prolonged incubation for 15 h at 60 °C.

with UV/VIS spectrophotometer. The HRP-containing amyloid hydrogel gave rise to the absorption maximum at 660 nm (Fig. 5B, solid line) while the CAF hydrogel treated with free HRP after the hydrogelation did not produce the blue product from TMB (Fig. 5B, dashed line), suggesting that free HRP was unable to permeate into the preformed CAF hydrogel made up of the nano-scaled pores. By the same reason, HRP once entrapped within the amyloid hydrogel could not escape freely either. The efficiency of HRP entrapment within the amyloid hydrogel was approximately 80% (Fig. S3).

Enzymatic sustainability of the entrapped HRP was evaluated by monitoring the blue product formation of TMB during 20 rounds of multiple enzyme catalyses (Fig. 5C, closed dots). It clearly indicated that the enzyme activity was retained for the most part during the multiple turnovers. Collagen-based hydrogel, however, did not allow the HRP to retain its activity during the repetitive reactions (Fig. 5C, open dots). The product formation of TMB by HRP dropped significantly even from the second reaction within the collagen hydrogel. The significant preservation of HRP activity within the amyloid hydrogel in comparison with the collagen-based gel was believed to be due to the huge difference on their pore sizes within the corresponding matrices as shown with the freeze-dried FE-SEM images (Fig. 5D). The large pore size of collagen-based gel at μm scale (31.5 μm in average) seemed to make it unsuitable for sheltering the enzyme inside (Fig. 5D, bottom) while the nano-spacing of the amyloid hydrogel allowed HRP to stay safe and stable during the multiple catalyses (Fig. 5D, top).

To evaluate protective effect of the amyloid hydrogel toward HRP against heat inactivation, themostability of the enzyme was investigated by incubating HRP at 60 °C present in a state of either free in solution or entrapped within the CAF hydrogel (Fig. 5E and F). The entrapped HRP was demonstrated to be resistant against the heat inactivation during initial 70 min of incubation by eliciting the decrease in activity by 12.5% at most while the free HRP lost its activity by more than 50% (Fig. 5E). Even after 15 h of extensive heat treatment at 60 °C, the HRP within the hydrogel lost its activity by approximately 20% while the activity of free HRP declined to more than 80% (Fig. 5F). Taken together, the amyloid hydrogel has been shown to be a suitable nanomatrix of protein fibrillar network for the enzyme entrapment in terms of sustaining the enzyme activity and providing a resistance barrier for HRP against the heat inactivation.

4. Discussion

We have demonstrated in this report that a single protein of α-synuclein exerts molecular-level polymorphism by generating two distinctive amyloid fibrils of SAF and CAF depending on the fibrillation processes. This would be one of a few examples producing the fibrillar polymorphism by altering the molecular assembly processes instead of influencing structural characteristics of individual amyloidogenic proteins with reaction conditions such as pH, temperature and small chemical ligands [4,33–39]. Different amyloidogenic process leads to the emergence of polymorphic amyloid fibrils with distinctive morphologies, which are attributed to their unique molecular-level structures. The ATR-FTIR data (Fig. 2E and F) could suggest that the predominant parallel β-sheet conformation of SAF might be transformed into the antiparallel β-sheet structure for CAF along with an alteration in other secondary structures of α-helix/random coil. It is, therefore, speculative that the antiparallel β-sheets connected by short loops could allow CAF to be bent in their morphology [40]. In addition, it could be considered that the alternative orientation of N- and C-termini within the antiparallel β-sheets would contribute to the stability of CAF over SAF.

The production of CAF through the membrane filtration procedure along with SAF via the agitated incubation supports our previous proposal that the amyloidogenesis of α-synuclein could be operated according to not only the prevalent nucleation-dependant fibrillation model [11] but also the double-concerted fibrillation model which includes the granular assembly process [15]. Once these polymorphs are generated, their unique characteristics can be transmitted to their progenies via the self-propagating mechanism [4], which allows us to have those morphologically and functionally unique protein nanofibrils in large quantities for various future applications including the enzyme entrapment shown in this study. Therefore, elucidation of the α-synuclein fibrillation mechanism and their fibrillar polymorphism provides us a potent strategy to produce the amyloid fibrils with unique structures exhibiting outstanding properties.

5. Conclusions

The production of morphologically distinctive and mechanically strong fibrils of CAF was achieved by the control of α-synuclein fibrillation process according to the double-concerted fibrillation model. Their self-propagating molecular-level polymorphism provided us with the CAF in a large quantity, which in turn leads to the superstructure of amyloid hydrogel shown to be suitable for the enzyme entrapment. In this respect, it is pertinent to consider that this nano-scaled three-dimensional protein fibrillar network could exert its potential to be employed in various areas of nano-biotechnology including tissue engineering, drug delivery, nano-filtration, and biosensor development.

Acknowledgements

This study was supported in part by a basic research program grant (R01-2007-000-20089-0) from Korea Science and Engineering Foundation and by another grant from the Seoul R&BD program (10538) through Institute of Bioengineering at SNU.

Appendix. Supporting information

Supporting information associated with this article can be found, in the online version, at doi:10.1016/j.biomaterials.2010.03.080.

Appendix

Figures with essential color discrimination. All the figures in this article have parts that are difficult to interpret in black and white. The full color images can be found in the online version at doi:10.1016/j.biomaterials.2010.03.080.

References

[1] Zhang S. Fabrication of novel biomaterials through molecular self-assembly. Nat Biotechnol 2003;21:1171–8.
[2] Tycko R. Molecular structure of amyloid fibrils: insights from solid-state NMR. Q Rev Biophys 2006;39:1–55.
[3] Sunde M, Blake CCF. From the globular to the fibrous state: protein structure and structural conversion in amyloid formation. Q Rev Biophys 1998;31:1–39.
[4] Petkova AT, Leapman RD, Guo Z, Yau W-M, Mattson MP, Tycko R. Self-propagating, molecular-level polymorphism in Alzheimer's β-amyloid fibrils. Science 2005;307:262–5.
[5] Chiti F, Dobson CM. Protein misfolding, functional amyloid, and human disease. Annu Rev Biochem 2006;75:333–66.
[6] Caughey B, Lansbury PT. Protofibrils, pores, fibrils and neurodegeneration: separating the responsible protein aggregates from the innocent bystanders. Annu Rev Neurosci 2003;26:267–98.
[7] Fowler DM, Koulov AV, Balch WE, Kelly JW. Functional amyloid – from bacteria to humans. Trends Biochem Sci 2007;32:217–24.
[8] Fowler DM, Koulov AV, Alory-Jost C, Marks MS, Balch WE, Kelly JW. Functional amyloid formation within mammalian tissue. PLoS Biol 2006;4:e6.
[9] Knowles TP, Fitzpatrick AW, Meehan S, Mott HR, Vendruscolo M, Dobson CM, et al. Role of intermolecular forces in defining material properties of protein nanofibrils. Science 2007;318:1900–3.

[10] Cherny I, Gazit E. Amyloids: not only pathological agents but also ordered nanomaterials. Angew Chem Int Ed 2008;47:4062–9.
[11] Jarrett JT, Lansbury PT. Seeding "one-dimensional crystallization" of amyloid: a pathogenic mechanism in Alzheimer's disease and scrapie? Cell 1993;73:1055–8.
[12] Harper JD, Lansbury PT. Models of amyloid seeding in Alzheimer's disease and scrapie: mechanistic truths and physiological consequences of the time-dependent solubility of amyloid proteins. Annu Rev Biochem 1997;66:385–407.
[13] Wood SJ, Wypych J, Steavenson S, Louis J-C, Citron M, Biere AL. α-Synuclein fibrillogenesis is nucleation-dependent. Implications for the pathogenesis of Parkinson's disease. J Biol Chem 1999;274:509–12.
[14] Kelly JW. Mechanisms of amyloidogenesis. Nat Struct Mol Biol 2000;7:824–6.
[15] Bhak G, Lee J-H, Hahn J-S, Paik SR. Granular assembly of α-synuclein leading to the accelerated amyloid fibril formation with shear stress. PLoS One 2009;4:e4177.
[16] Spillantini MG, Schmidt ML, Lee VM-Y, Trojanowski JQ, Jakes R, Goedert M. α-Synuclein in Lewy bodies. Nature 1997;388:839–40.
[17] Clayton DF, George JM. The synucleins: a family of proteins involved in synaptic function, plasticity, neurodegeneration and disease. Trends Neurosci 1998;21:249–54.
[18] Maiti NC, Apetri MM, Zagorski MG, Carey PR, Anderson VE. Raman spectroscopic characterization of secondary structure in natively unfolded proteins: α-synuclein. J Am Chem Soc 2004;126:2399–408.
[19] Conway KA, Harper JD, Lansbury PT. Fibrils formed in vitro from α-synuclein and two mutant forms linked to Parkinson's disease are typical amyloid. Biochemistry 2000;39:2552–63.
[20] Hashimoto M, Hsu LJ, Sisk A, Xia Y, Takeda A, Sundsmo M, et al. Human recombinant NACP/α-synuclein is aggregated and fibrillated in vitro: relevance for Lewy body disease. Brain Res 1998;799:301–6.
[21] Lee J-H, Bhak G, Lee S-G, Paik SR. Instantaneous amyloid fibril formation of α-synuclein from the oligomeric granular structures in the presence of hexane. Biophys J 2008;95:L16–8.
[22] Paik SR, Lee J-H, Kim D-H, Chang C-S, Kim J. Aluminum-induced structural alterations of the precursor of the non-Aβ component of Alzheimer's disease amyloid. Arch Biochem Biophys 1997;344:325–34.
[23] Rivetti C, Guthold M, Bustamante C. Scanning force microscopy of DNA deposited onto mica: equilibration versus kinetic trapping studied by statistical polymer chain analysis. J Mol Biol 1996;264:919–32.
[24] Doi M, Edwards SF. The theory of polymer dynamics. Oxford: Oxford Univ Press; 1986.
[25] Gosal WS, Morten IJ, Hewitt EW, Smith DA, Thomson NH, Radford SE. Competing pathways determine fibril morphology in the self-assembly of β2-microglobulin into amyloid. J Mol Biol 2005;351:850–64.
[26] Kim S, Chu C-C. Pore structure analysis of swollen dextran-methacrylate hydrogels by SEM and mercury intrusion porosimetry. J Biomed Mater Res 2000;53:258–66.
[27] Berthelot K, Immel F, Géan J, Lecomte S, Oda R, Kauffmann B, et al. Driving amyloid toxicity in a yeast model by structural change: a molecular approach. Faseb J 2009;23:1–10.
[28] Cordeiro Y, Kraineva J, Ravindra R, Lima LMTR, Gomes MPB, Foguel D, et al. Hydration and packing effects on prion folding and β-sheet conversion. J Biol Chem 2004;279:32354–9.
[29] Zurdo J, Guijarro JI, Jiménez JL, Saibil HR, Dobson CM. Dependence on solution conditions of aggregation and amyloid formation by an SH3 domain. J Mol Biol 2001;311:325–40.
[30] Kammerer RA, Kostrewa D, Zurdo J, Detken A, García-Echeverría C, Green JD, et al. Exploring amyloid formation by a de novo design. Proc Natl Acad Sci U S A 2004;101:4435–40.
[31] Valéry C, Paternostre M, Robert B, Gulik-Krzywicki T, Narayanan T, Dedieu J-C, et al. Biomimetic organization: octapeptide self-assembly into nanotubes of viral capsid-like dimension. Proc Natl Acad Sci U S A 2003;100:10258–62.
[32] Ehrick JD, Deo SK, Browning TW, Bachas LG, Madou MJ, Daunert S. Genetically engineered protein in hydrogels tailors stimuli-responsive characteristics. Nat Mater 2005;4:298–302.
[33] Verel R, Tomka IT, Bertozzi C, Cadalbert R, Kammerer RA, Steinmetz MO, et al. Polymorphism in an amyloid-like fibril-forming model peptide. Angew Chem, Int Ed 2008;47:5842–5.
[34] Griffin MDW, Mok MLY, Wilson LM, Pham CLL, Waddington LJ, Perugini MA, et al. Phospholipid interaction induces molecular-level polymorphism in apolipoprotein C-II amyloid fibrils via alternative assembly pathways. J Mol Biol 2008;375:240–56.
[35] Kodali R, Wetzel R. Polymorphism in the intermediates and products of amyloid assembly. Curr Opin Struct Biol 2007;17:48–57.
[36] Radovan D, Smirnovas V, Winter R. Effect of pressure on islet amyloid polypeptide aggregation: revealing the polymorphic nature of the fibrillation process. Biochemistry 2008;47:6352–60.
[37] Pedersen JS, Dikov D, Flink JL, Hjuler HA, Christiansen G, Otzen DE. The changing face of glucagon fibrillation: structural polymorphism and conformational imprinting. J Mol Biol 2006;355:501–23.
[38] Paravastu AK, Petkova AT, Tycko R. Polymorphic fibril formation by residues 10–40 of the Alzheimer's β-amyloid peptide. Biophys J 2006;90:4618–29.
[39] Goldsbury C, Frey P, Olivieri V, Aebi U, Müller SA. Multiple assembly pathways underlie amyloid-β fibril polymorphisms. J Mol Biol 2005;352:282–98.
[40] Emberly EG, Mukhopadhyay R, Tang C, Wingreen NS. Flexibility of β-sheets: principal component analysis of database protein structures. Proteins 2004;55:91–8.